

Enhanced Connectivity in Ambient Backscatter Communications via Fluid Antenna Readers

Masoud Kaveh[†], Farshad Rostami Ghadi[§], Riku Jäntti[†], Kai-Kit Wong[‡], F. Javier Lopez-Martinez[§]

[†]Department of Information and Communications Engineering, Aalto University, Espoo, Finland

[§]Department of Signal Theory, Networking and Communications, University of Granada, Granada, Spain.

[‡]Department of Electronic and Electrical Engineering, University College London, London, U.K.

Abstract—Ambient backscatter communication (AmBC) enables ultra-low-power connectivity by allowing passive backscatter devices (BDs) to convey information through reflection of ambient signals. However, the cascaded AmBC channel suffers from severe double path loss and multiplicative fading, while accurate channel state information (CSI) acquisition is highly challenging due to the weak backscattered signal and the resource-limited nature of BDs. To address these challenges, this paper considers an AmBC system in which the reader is equipped with a pixel-based fluid antenna system (FAS). By dynamically selecting one antenna position from a dense set of pixels within a compact aperture, the FAS-enabled reader exploits spatial diversity through measurement-driven port selection, without requiring explicit CSI acquisition or multiple RF chains. The intrinsic rate-energy tradeoff at the BD is also incorporated by jointly optimizing the backscatter modulation coefficient under an energy harvesting (EH) neutrality constraint. To efficiently solve this problem, a particle swarm optimization (PSO)-based framework is developed to jointly determine the FAS port selection and modulation coefficient on an optimize-then-average (OTA) basis. Simulation results show that the proposed scheme significantly improves the achievable rate compared with conventional single-antenna readers, with gains preserved under imperfect observations, stringent EH constraints, and different pixel spacings.

Index Terms—Ambient backscatter communication, Internet of Things, fluid antenna systems, particle swarm optimization.

I. INTRODUCTION

AMBIENT backscatter communication (AmBC) has emerged as a key enabling technology for ultra-low-power and battery-less connectivity in large-scale Internet-of-Things (IoT) networks [1], [2]. By modulating and reflecting incident radio-frequency (RF) signals instead of generating new waveforms, backscatter devices (BDs) can operate with minimal energy consumption and hardware complexity [3], [4]. Despite these advantages, AmBC performance is fundamentally limited by the cascaded channel formed by source-to-BD and BD-to-reader links. The resulting double path loss and multiplicative fading cause severe signal attenuation, which significantly constrains AmBC coverage and reliability [5], [6]. In addition, acquiring accurate instantaneous channel state information (CSI) is particularly challenging due to the extremely weak backscattered signal and the inability of passive BDs to support explicit channel training [7], [8].

Recent studies have explored fluid antenna systems (FAS) [9], [10] as an effective means of mitigating channel impair-

ments in backscatter and energy-constrained wireless systems [11]–[13]. Early analytical works show that antenna position flexibility at the reader can significantly improve outage performance and reliability in backscatter communications (BC) under spatially correlated fading, confirming the diversity gains of FAS over conventional fixed-antenna readers [11]. Related studies have extended FAS concepts to wireless powered systems, demonstrating notable improvements in outage probability, secrecy performance, and achievable capacity when a single FAS port is optimally selected [12], [13].

Despite the promising performance gains reported in [11]–[13], existing FAS-aided backscatter studies predominantly rely on idealized assumptions, such as analytically tractable fading models and perfect or statistical channel knowledge. In particular, the effect of channel gain observation uncertainty, an inherent characteristic of AmBC arising from the extremely weak backscattered signal and the absence of explicit channel training at passive BDs, has received little attention. Furthermore, prior works typically decouple communication design from the energy harvesting (EH) requirements of the BD by assuming fixed or unconstrained reflection coefficients. In practical AmBC deployments, however, the BD must sustain its operation through harvested energy while simultaneously enabling reliable information transfer, giving rise to an intrinsic rate–energy tradeoff that directly impacts system performance [14], [15]. These considerations expose a clear gap between existing analytical FAS performance characterizations and the development of robust, implementable antenna selection strategies suited to realistic AmBC conditions.

Motivated by this gap, this paper investigates an AmBC system in which the reader is equipped with a pixel-based FAS to enhance the cascaded backscatter channel under practical operating constraints. Instead of assuming perfect CSI, antenna port selection is performed based solely on noisy observations of the cascaded channel gains. To explicitly account for energy sustainability at the BD, we formulate a reader-centric optimization problem that maximizes the achievable rate by jointly optimizing the FAS port selection and the backscatter modulation coefficient under an EH constraint. Owing to the nonconvex nature of the resulting problem, a particle swarm optimization (PSO)-based framework is developed that operates directly on observed channel gains. Simulation results

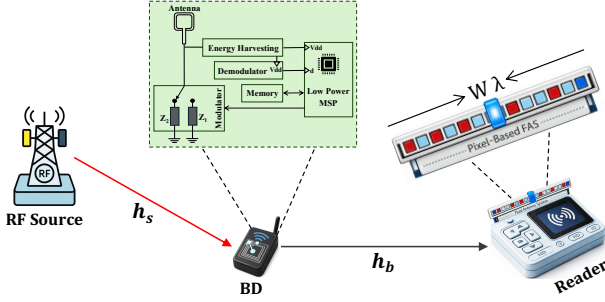


Fig. 1. The considered AmBC system with pixel-based FAS at the reader.

confirm that the proposed FAS-enabled reader consistently outperforms traditional fixed-antenna benchmarks across a wide range of operating conditions.

II. SYSTEM MODEL

We consider an AmBC setup consisting of an RF source (illuminator), a single-antenna passive BD, and a reader equipped with a pixel-based FAS, as illustrated in Fig. 1. The RF source continuously transmits an unmodulated carrier (or a known waveform) with transmit power P_s . The BD harvests energy from the incident RF signal and conveys information by switching its load impedance between two states, corresponding to binary backscatter modulation [16], [17]. The reader employs the FAS to activate one antenna port (pixel) at a time from a set of K preset ports distributed over a linear aperture of length $W\lambda$, where λ denotes the carrier wavelength and W is the normalized FAS size. The K FAS ports are uniformly spaced along the aperture with sub-wavelength inter-port distance d [18].

Let $h_s \in \mathbb{C}$ denote the forward channel from the RF source to the BD, and $h_{b,k} \in \mathbb{C}$ denote the backscatter channel from the BD to the k -th FAS port at the reader, where $k \in \{1, \dots, K\}$. The corresponding channel power gains are defined as

$$g_s \triangleq |h_s|^2, \quad g_{b,k} \triangleq |h_{b,k}|^2. \quad (1)$$

Due to the finite aperture of the FAS, the backscatter channels $\{h_{b,k}\}$ are spatially correlated. A commonly adopted correlation model is the Jakes' correlation across antenna ports, given by

$$\mathbf{R} = [\rho_{k,\ell}], \quad \rho_{k,\ell} = J_0\left(2\pi \frac{|k-\ell|}{K-1} W\right), \quad (2)$$

where $J_0(\cdot)$ denotes the zero-order Bessel function of the first kind, and $\rho_{k,\ell}$ represents the spatial correlation coefficient between the k -th and ℓ -th FAS ports.

Then, the RF signal received at the BD is expressed as

$$r_{\text{BD}} = \sqrt{P_s} h_s x + n_{\text{BD}}, \quad (3)$$

where x is the unit-power transmitted waveform, i.e., $\mathbb{E}[|x|^2] = 1$, and n_{BD} denotes the receiver noise at the BD, which is typically negligible compared to the incident carrier for passive operation [6], [19]. The BD modulates information by switching its load impedance, thereby changing its reflection

coefficient. Let Γ_i denote the reflection coefficient associated with impedance state Z_i , $i \in \{0, 1\}$ [20]. For binary signaling, the reflection coefficient selected by the BD is

$$\Gamma(b) = \begin{cases} \Gamma_0, & b = 0, \\ \Gamma_1, & b = 1, \end{cases} \quad (4)$$

where $b \in \{0, 1\}$ denotes the information bit. In this work, we consider ON-OFF keying (OOK) backscatter modulation [21], where the *OFF* state ($b = 0$) corresponds to a matched load with negligible reflection, and the *ON* state ($b = 1$) corresponds to a mismatched load that reflects a portion of the incident RF signal. The backscatter modulation coefficient is defined as

$$\alpha(b) \triangleq \sqrt{\eta} \Gamma(b), \quad (5)$$

where $\eta \in (0, 1]$ accounts for the reflection efficiency of the BD, capturing losses due to impedance mismatch and non-ideal reradiation.

Consequently, the received baseband signal at the k -th FAS port is modeled as

$$y_k = \sqrt{P_s} h_s h_{b,k} \alpha(b) x + z_k, \quad (6)$$

where $z_k \sim \mathcal{CN}(0, \sigma^2)$ is additive white Gaussian noise (AWGN) at the reader. Accordingly, the cascaded end-to-end channel observed at the k -th port is

$$h_{c,k} \triangleq h_s h_{b,k}, \quad g_{c,k} \triangleq |h_{c,k}|^2 = g_s g_{b,k}. \quad (7)$$

The pixel-based FAS at the reader is equipped with a single RF chain and can activate only one antenna port at a time. Due to the passive nature of the BD and the extremely weak backscattered signal, acquiring accurate instantaneous channel state information (CSI) is highly challenging in AmBC systems. Therefore, rather than assuming perfect CSI or performing explicit channel estimation, the reader adopts a measurement-driven port selection strategy based on noisy observations of the port quality, which are obtained through short-term measurements of received signal-to-noise ratio (SNR). Specifically, the observed cascaded gain at the k -th port is modeled as

$$\tilde{g}_{c,k} = g_{c,k} (1 + \delta_k), \quad (8)$$

where $\delta_k \sim \mathcal{N}(0, \sigma_\delta^2)$ models the relative uncertainty in the observed port quality due to noisy power/SNR measurements of the cascaded channel [22]. This model reflects a measurement-driven observation process rather than classical channel estimation, and captures imperfect channel knowledge at the reader without assuming access to instantaneous CSI. Then, the reader selects the FAS port according to

$$k^* = \arg \max_{k \in \{1, \dots, K\}} \tilde{g}_{c,k}, \quad (9)$$

which yields the effective cascaded channel gain

$$g_{\text{FAS}} \triangleq g_{c,k^*}. \quad (10)$$

The post-selection received signal at the reader is given by

$$y = \sqrt{P_s} h_{c,k^*} \alpha(b) x + z, \quad (11)$$

where $z \sim \mathcal{CN}(0, \sigma^2)$ denotes AWGN.

Conditioned on the selected FAS port and the backscatter coefficient, the instantaneous SNR at the reader is

$$\gamma = \frac{P_s |\alpha(b)|^2 g_{\text{FAS}}}{\sigma^2}. \quad (12)$$

Accordingly, the achievable backscatter rate is expressed as

$$R = \log_2(1 + \gamma), \quad (13)$$

which serves as an upper-bound performance metric commonly adopted to evaluate relative gains under different antenna and observation configurations.

In addition to information transfer, the BD harvests energy from the incident RF signal. The average RF power impinging on the BD antenna is proportional to $P_s g_s$. Since AmBC relies on reflecting a portion of the incident signal, the harvested and backscattered powers originate from the same RF source and therefore compete for the available energy at the BD. To capture this trade-off, an EH model is adopted [23], where the harvested DC power is given by

$$P_{\text{EH}} = \xi(1 - |\alpha(b)|^2)P_s g_s, \quad (14)$$

with $\xi \in (0, 1]$ denoting the RF-to-DC conversion efficiency. To ensure energy-neutral operation of the BD, the harvested power must satisfy

$$P_{\text{EH}} \geq P_c, \quad (15)$$

where P_c denotes the circuit power consumption associated with sensing, logic, and impedance switching.

III. PROBLEM FORMULATION

In this section, we formulate the joint optimization problem for the considered pixel-based FAS-enabled AmBC system. Our objective is to maximize the achievable backscatter rate by jointly optimizing the backscatter modulation coefficient at the BD and the antenna port selection at the FAS-equipped reader, while accounting for imperfect CSI and ensuring energy-neutral operation of the BD.

The first optimization variable is the non-zero backscatter modulation level $a_1 \triangleq |\alpha(1)|^2$, corresponding to the *ON* reflection state of the BD, where $a_0 = |\alpha(0)|^2 = 0$, and the second is the selected FAS port index $k \in \{1, \dots, K\}$ at the reader. For practical backscatter hardware, the modulation level a_1 is constrained to a feasible interval [24]

$$a_{\min} \leq a_1 \leq a_{\max} \leq 1, \quad (16)$$

where a_{\min} ensures a detectable backscattered signal and a_{\max} is determined by circuit and impedance design limitations.

As established earlier, due to imperfect CSI, the reader relies on noisy observations of the cascaded channel gains. Let $\tilde{g}_{c,k}$ denote the observed cascaded gain at port k (cf. (8)), and denote by g_{FAS} the effective (true) cascaded gain of the selected port. For a given pair (k, a_1) , the instantaneous rate is written as $R(k, a_1)$, where the dependence on imperfect CSI is captured through the observation-driven decision on k . Assuming binary backscatter modulation with $\Pr(b = 1) = p_1$

and $\Pr(b = 0) = 1 - p_1$, the instantaneous SNR follows directly from (12), and thus $R(k, a_1)$ serves as the objective function to be maximized.

On the other hand, the BD must satisfy an energy sustainability constraint to maintain passive operation. Under the adopted linear EH model in (14), we impose an EH margin constraint to ensure robust operation under channel fluctuations, given by

$$\xi(1 - p_1 a_1)P_s g_s \geq \mu P_c \quad (17)$$

where $\mu > 1$ is a prescribed EH margin factor.

To be consistent with practical operation under imperfect CSI, we adopt an optimize-then-average (OTA) performance metric. Specifically, for each channel realization and observation-noise sample, the reader selects a port based on the observed gains and the design variables, and the achieved rate is then averaged across realizations. Accordingly, the joint OTA optimization problem is formulated as

$$\max_{a_1, k} \mathbb{E}[R(a_1, k^*)] \quad (18a)$$

$$\text{s.t. } \xi(1 - p_1 a_1)P_s g_s \geq \mu P_c, \quad (18b)$$

$$a_{\min} \leq a_1 \leq a_{\max}, \quad (18c)$$

$$k \in \{1, \dots, K\}. \quad (18d)$$

Problem (18) is non-convex and involves mixed discrete-continuous optimization due to the discrete FAS port index and the coupled dependence of the achievable rate and harvested energy on the backscatter modulation coefficient. While the reflection coefficient can be optimized in closed form under EH constraints for a selected port, the port-selection variable renders the problem nonconvex and combinatorial. To efficiently handle this structure under imperfect CSI, we adopt a PSO-based solution to efficiently solve this problem. To that aim, each particle i maintains a position vector

$$\mathbf{x}_i = [u_i, a_{1,i}], \quad (19)$$

where $u_i \in [1, K]$ is a continuous surrogate variable that is decoded to the discrete FAS port index as $k_i = \text{clip}([u_i], 1, K)$, and $a_{1,i} \in [a_{\min}, a_{\max}]$ denotes the candidate ON-level backscatter modulation coefficient. This encoding enables joint optimization of the reader-side port selection and the BD-side reflection strength within a unified search space.

At iteration t , the velocity and position of particle i are updated according to

$$\mathbf{v}_i^{(t+1)} = \omega \mathbf{v}_i^{(t)} + c_1 r_1 (\mathbf{x}_{i,\text{best}} - \mathbf{x}_i^{(t)}) + c_2 r_2 (\mathbf{x}_{\text{best}} - \mathbf{x}_i^{(t)}), \quad (20)$$

$$\mathbf{x}_i^{(t+1)} = \Pi_{\mathcal{X}} \left(\mathbf{x}_i^{(t)} + \mathbf{v}_i^{(t+1)} \right), \quad (21)$$

where ω is the inertia weight, c_1 and c_2 are the cognitive and social learning coefficients, and $r_1, r_2 \sim \mathcal{U}(0, 1)$. The projection operator $\Pi_{\mathcal{X}}(\cdot)$ enforces feasibility by ensuring $u_i \in [1, K]$, $a_{1,i} \in [a_{\min}, a_{\max}]$, and satisfaction of the energy-neutrality constraint in (18b).

For each particle realization, the decoded port index k_i determines the FAS port selected at the reader based on the

Algorithm 1 PSO for Pixel-Based FAS-aided AmBC

Require: $K, N, N_p, T, (\omega, c_1, c_2), (P_s, \sigma^2, \xi, P_c, p_1, \epsilon), \sigma_\delta^2, (a_{\min}, a_{\max})$.
Ensure: Best solution (k^*, a_1^*) and \bar{R}_{OTA}^* .

- 1: **for** $n = 1$ to N **do**
- 2: Generate one channel realization and observation noise; form $\{\tilde{g}_{c,k}\}_{k=1}^K$.
- 3: Initialize particles $\mathbf{x}_i = [u_i, a_{1,i}]$ with $u_i \in [1, K]$, $a_{1,i} \in [a_{\min}, a_{\max}]$.
- 4: **for** $t = 1$ to T **do**
- 5: **for** each particle i **do**
- 6: Decode $k_i \leftarrow \text{clip}(\lfloor u_i \rfloor, 1, K)$ and set candidate $a_{1,i}$.
- 7: If (18b) is violated, discard particle (infeasible);
- 8: Otherwise compute instantaneous rate as fitness.
- 9: Update personal and global bests.
- 10: **end for**
- 11: Update particle velocities and positions;
- 12: Project onto feasible ranges.
- 13: **end for**
- 14: Record the optimized $R^{*(n)}$ with (k^*, a_1^*) for realization n .
- 15: **end for**
- 16: Compute $\bar{R}_{\text{OTA}}^* = \frac{1}{N} \sum_{n=1}^N R^{*(n)}$.
- 17: **return** (k^*, a_1^*) and \bar{R}_{OTA}^* .

noisy cascaded gain observations. The instantaneous backscatter rate corresponding to $(k_i, a_{1,i})$ is then evaluated and used as the particle fitness. Personal and global best solutions are updated accordingly. After convergence, the PSO yields the optimized solution (k^*, a_1^*) , whose performance is assessed using the OTA rate metric. Algorithm 1 illustrates the PSO-driven optimization process in this paper.

IV. RESULTS AND DISCUSSIONS

A. Simulation Setup

We consider a dense pixel-based FAS at the reader with sub-wavelength inter-port spacing $d = \lambda/8$, which enables a compact antenna aperture and strong spatial correlation among ports. The carrier frequency is set to $f_c = 3.5$ GHz, corresponding to a wavelength $\lambda \approx 0.0857$ m. The FAS consists of $K \in \{5, 10, 20\}$ uniformly spaced ports over a linear aperture of length $W\lambda$, where $W = (K-1)d/\lambda$. The RF source continuously transmits an unmodulated carrier with a maximum transmit power $P_s = 20$ dbm. The noise power at the reader is set to $\sigma^2 = -100$ dBm and the circuit power consumption of the BD is $P_c = -20$ dBm. For imperfect observation modeling, the variance of the relative channel gain observation error is set to $\sigma_\delta^2 = 0.05$, corresponding to a moderate level of measurement uncertainty in the observed cascaded channel gain. Large-scale path loss between the RF source, the BD, and the reader follows $L(d) = d^{-\chi}$, where $\chi = 2.9$ denotes the path-loss exponent. The forward (source-to-B)D and backscatter (BD-to-FAS) channels incorporate both large-scale attenuation and small-scale fading, which is modeled as spatially correlated Rician fading with the backscatter channel $\mathbf{h}_b = [h_{b,1}, \dots, h_{b,K}]^\top$ is generated as

$$\mathbf{h}_b = \sqrt{\frac{\kappa}{\kappa+1}} \mathbf{h}_{\text{LOS}} + \sqrt{\frac{1}{\kappa+1}} \mathbf{R}^{1/2} \mathbf{w}, \quad (22)$$

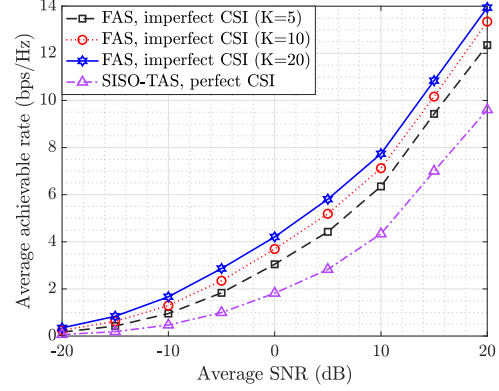


Fig. 2. Average achievable rate versus average SNR for the proposed FAS-based AmBC with different number of preset positions.

where $\kappa = 5$ is the Rician factor, $\mathbf{w} \sim \mathcal{CN}(\mathbf{0}, \mathbf{I})$, and \mathbf{R} is the spatial correlation matrix constructed using the Jakes' model in (2). The matrix square root $\mathbf{R}^{1/2}$ is obtained via Cholesky factorization. The forward channel h_s is modeled independently with the same Rician factor.

The OFF state in BD's OOK modulation corresponds to $\alpha(0) \approx 0$, while the ON state is characterized by $\alpha(1) = \sqrt{a_1}$, where $a_1 \in [a_{\min}, a_{\max}]$ is optimized subject to the energy-neutrality constraint. Unless otherwise stated, the bit probability is set to $p_1 = \Pr(b = 1) = 0.5$. The reflection efficiency is fixed to $\eta = 0.8$, and the RF-to-DC conversion efficiency is set to $\xi = 0.6$. All performance metrics are computed using the OTA approach by averaging over $N = 10^5$ independent channel and observation-noise realizations. The PSO algorithm employs a swarm of $N_p = 50$ particles and runs for $T = 50$ iterations. The inertia weight is set to $\omega = 0.6$, and the cognitive and social learning coefficients are chosen as $c_1 = c_2 = 1.2$. As a benchmark, we consider a traditional antenna system (TAS) reader equipped with a single antenna, where perfect CSI in a single-input single-output (SISO) AmBC system is assumed to be provided at the reader.

B. Result Analysis and Discussion

Fig. 2 plots the average achievable rate versus the average received SNR and highlights the clear advantage of the proposed pixel-based FAS under imperfect CSI relative to the SISO-TAS benchmark even with perfect CSI. Across the full SNR range, the FAS curves remain above TAS, showing that the spatial selectivity gained by switching among multiple ports provides a diversity benefit that outweighs occasional port-misselection under noisy channel observations. The performance improves steadily with the number of candidate ports, with $K = 20$ outperforming $K = 10$ and $K = 5$ at all SNRs, because a larger port set increases the chance of encountering a favorable cascaded-channel realization and thus raises the effective selected gain. At low SNR, the curves are relatively close since noise dominates and selection diversity

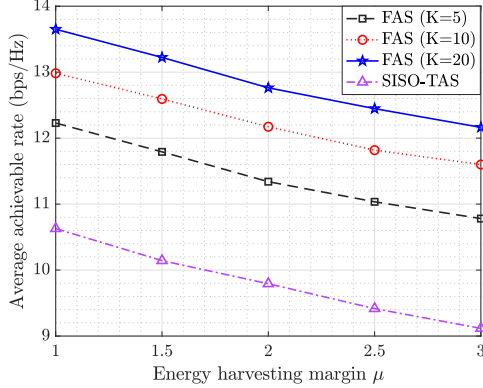


Fig. 3. Average achievable rate versus average SNR for the proposed FAS-based AmBC with different number of preset positions.

has limited impact; at moderate and high SNR, the achievable rate becomes more sensitive to the selected cascaded gain inside $\log_2(1 + \gamma)$, so the gap between FAS and TAS, as well as the separation among different K , becomes more visible.

Fig. 3 illustrates the impact of the EH safety margin μ on the average achievable rate for the proposed pixel-based FAS AmBC. As μ increases, the harvested energy requirement at BD becomes more stringent, which directly tightens the feasible reflection coefficient and reduces the portion of incident power available for backscatter modulation. This effect leads to a monotonic degradation in achievable rate for all schemes. Despite this increasingly conservative energy constraint, the pixel-FAS consistently maintains a clear performance advantage over the TAS benchmark across the entire range of μ , highlighting the robustness of spatial diversity even when energy availability is constrained. Moreover, increasing the number of FAS pixels yields a systematic rate improvement, as larger K provides a higher probability of selecting a favorable backscatter path under imperfect CSI. The parallel downward trends observed for all configurations confirm that the safety margin primarily governs the energy-rate tradeoff, while the relative ordering of the curves demonstrates that the gains from pixel-level spatial selection remain effective under strict EH requirements.

Fig. 4 illustrates the impact of channel gain observation error variance on the average achievable rate. For very small error variance, the achievable rate of all FAS configurations remains nearly constant, indicating that pixel selection based on the observed cascaded channel gains is reliable when the gain observation is sufficiently accurate. As the observation error variance increases beyond approximately 10^{-3} , a clear degradation in achievable rate is observed for all FAS cases. This degradation becomes more pronounced as the number of pixels K increases, since a larger candidate set amplifies the probability of incorrect pixel selection when the gain observations are noisy. In contrast, the SISO-TAS benchmark exhibits almost invariant performance over the entire range of error variance, as no antenna or pixel selection is involved and

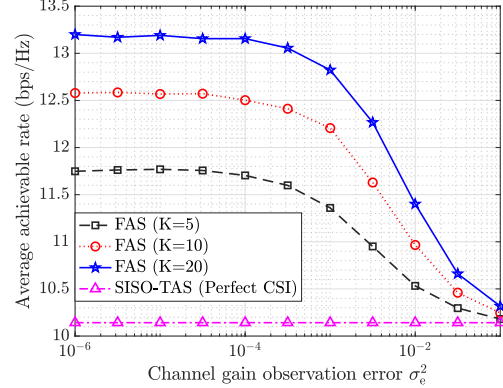


Fig. 4. Average achievable rate versus CSI error variance for the proposed FAS-based AmBC with different number of preset positions.

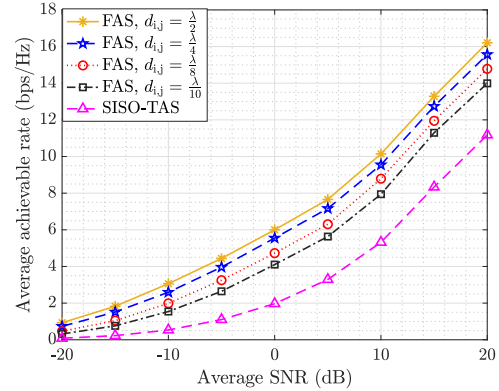


Fig. 5. Average achievable rate versus average received SNR for the pixel-based FAS-aided AmBC with $K = 10$ and different inter-pixel spacings $d_{i,j}$.

the received signal depends only on the true channel realization. Despite its sensitivity to gain observation uncertainty, the pixel-based FAS scheme consistently outperforms the SISO-TAS benchmark across a wide range of error levels. This confirms that the spatial diversity offered by multiple pixels provides a substantial rate advantage that outweighs the adverse effects of imperfect gain observation, except in regimes where the observation noise becomes severely dominant.

Fig. 5 depicts the average achievable rate as a function of the average received SNR for the proposed pixel-based FAS scheme under different inter-pixel spacings $d_{i,j}$. Several clear trends can be observed. First, for all SNR values, pixel-based FAS consistently outperforms the SISO-TAS reader, confirming the substantial spatial diversity and aperture gains offered by multi-pixel structures even without conventional antenna arrays. Second, increasing the inter-pixel spacing leads to a systematic improvement in achievable rate, with the case $d_{i,j} = \lambda/2$ providing the highest performance across the entire SNR range. This behavior stems from the reduced spatial correlation and the effective enlargement of the electromagnetic aperture, which together enhance the probability

of selecting a pixel with a strong cascaded channel gain. At moderate and high SNR regimes, the performance gap between different spacings becomes more pronounced, highlighting the increasing importance of spatial separation when the system is not noise-limited. However, the results also indicate that enlarging the pixel spacing for a fixed operating bandwidth and physical surface size does not lead to unbounded rate improvements. Beyond a certain spacing, the achievable rate exhibits a saturation behavior, as the benefits from further correlation reduction diminish while path-loss, finite aperture constraints, and channel hardening effects dominate. This observation suggests that there exists an optimal spacing region that balances spatial diversity and practical surface constraints, rather than a monotonic benefit from arbitrarily increasing the inter-pixel distance.

V. CONCLUSION

This paper studied a pixel-based FAS architecture for AmBC receivers operating under practical EH and channel uncertainty constraints. By exploiting antenna position flexibility within a compact aperture, the proposed FAS-enabled reader was able to mitigate the severe impairments caused by cascaded double path loss and multiplicative fading without increasing the number of RF chains or violating the low-power nature of AmBC. The joint optimization of the FAS port selection and the backscatter modulation level was formulated as a mixed discrete-continuous problem under an EH safety margin. Due to the nonconvex structure of the problem and the presence of imperfect channel gain observations, a PSO framework was developed to efficiently identify near-optimal solutions. The OTA performance metric was adopted to reflect practical operation, where decisions are made based on noisy observations and performance is averaged over channel realizations. Simulation results showed that the proposed FAS-enabled AmBC consistently outperformed a conventional single-antenna reader across a broad range of system parameters, while maintaining robustness against observation errors and stringent energy constraints. The results further illustrated the inherent tradeoff between spatial diversity, energy availability, and aperture utilization, revealing that while increased spatial resolution improves performance, the achievable gains saturate for a fixed physical surface.

ACKNOWLEDGMENT

This work has received funding from the SNS JU under the EU's Horizon Europe research and innovation programme under Grant Agreement No. 101192113 (Ambient-6G), the EU's Horizon 2022 Research and Innovation Programme under Marie Skłodowska-Curie Grant No. 101107993, and by grant PID2023-149975OB-I00 (COSTUME) funded by MICIU/AEI/10.13039/501100011033 and by FEDER/UE.

REFERENCES

- [1] M. A. Jamshed, et al., "Artificial intelligence, ambient backscatter communication and non-terrestrial networks: A 6G commixture," *IEEE Internet of Things Magazine*, vol. 8, no. 2, pp. 88–94, 2025.
- [2] J. Liao, et al., "Ambient backscatter communication in LTE uplink using sounding reference signals," *IEEE Internet of Things Journal*, vol. 12, no. 23, pp. 50785–50800, Dec. 2025.
- [3] M. Kaveh, F. R. Ghadi, Y. Zhang, Z. Yan, and R. Jäntti, "Voltage profile-driven physical layer authentication for RIS-aided backscattering tag-to-tag networks," *IEEE Internet of Things Journal*, Vol. 12, no. 23, pp. 51099–51113, 2025.
- [4] Y. Zhang, et al., "Artificial noise management for securing backscatter communication networks: Current advances, open challenges, and future directions," *IEEE Network*, doi: 10.1109/MNET.2025.3570547, 2025.
- [5] B. Gu, D. Li, H. Ding, G. Wang, and C. Tellambura, "Breaking the interference and fading gridlock in backscatter communications: State-of-the-art, design challenges, and future directions," *IEEE Communications Surveys & Tutorials*, vol. 27, no. 2, pp. 870–911, Apr. 2025.
- [6] M. Kaveh, F. R. Ghadi, Z. Li, Z. Yan, and R. Jäntti, "Secure backscatter communications through RIS: Modeling and performance," *IEEE Transactions on Vehicular Technology*, doi: 10.1109/TVT.2025.3612485, 2025.
- [7] H. Guo, Q. Zhang, S. Xiao, and Y.-C. Liang, "Exploiting multiple antennas for cognitive ambient backscatter communication," *IEEE Internet of Things Journal*, vol. 6, no. 1, pp. 765–775, Feb. 2019.
- [8] S. Ma, G. Wang, R. Fan, and C. Tellambura, "Blind channel estimation for ambient backscatter communication systems," *IEEE Communications Letters*, vol. 22, no. 6, pp. 1296–1299, Jun. 2018.
- [9] K. K. Wong, A. Shojaeifard, K. F. Tong, and Y. Zhang, "Fluid antenna systems," *IEEE Trans. Wireless Commun.*, vol. 20, pp. 1950–1962, 2021.
- [10] W. K. New, et al., "A tutorial on fluid antenna system for 6G networks: Encompassing communication theory, optimization methods and hardware designs," *IEEE Commun. Surv. Tutor.*, vol. 27, pp. 2325–2377, 2025.
- [11] F. R. Ghadi, M. Kaveh, K.-K. Wong, and Y. Zhang, "Performance analysis of FAS-aided backscatter communications," *IEEE Wireless Communications Letters*, vol. 13, no. 9, pp. 2412–2416, Sep. 2024.
- [12] F. R. Ghadi, M. Kaveh, K.-K. Wong, R. Jäntti, and Z. Yan, "On performance of FAS-aided wireless powered NOMA communication systems," in *Proc. IEEE 20th Int. Conf. Wireless and Mobile Computing, Networking and Communications (WiMob)*, pp. 496–501, 2024.
- [13] F. R. Ghadi, M. Kaveh, K.-K. Wong, D. Martín, R. Jäntti, and Z. Yan, "Physical layer security in FAS-aided wireless powered NOMA systems," *Computer Communications*, Art. no. 108274, 2025.
- [14] P. Ghosh, S. Dhar Roy, and S. Kundu, "Energy harvesting-assisted two-user cooperative NOMA with ambient backscattering," *International Journal of Communication Systems*, vol. 38, no. 4, p. e6133, 2025.
- [15] M. Kaveh, F. R. Ghadi, R. Jäntti, and Z. Yan, "Secrecy performance analysis of backscatter communications with side information," *Sensors*, vol. 23, no. 20, p. 8358, 2023.
- [16] N. Barbot and M. Reynolds, "A general receiver for backscatter signals: A step-by-step tutorial," *IEEE Microwave Magazine*, vol. 27, no. 2, pp. 62–74, Feb. 2026.
- [17] M. Kaveh, F. R. Ghadi, Z. Yan, and R. Jäntti, "RIS-aided backscattering tag-to-tag networks: Performance analysis," in *Proc. IEEE Int. Mediterranean Conf. Commun. and Networking (MeditCom)*, Nice, France, Jun. 2025, pp. 1–6.
- [18] F. R. Ghadi, et al., "Copula-based performance analysis for fluid antenna systems under arbitrary fading channels," *IEEE Communications Letters*, vol. 27, no. 11, pp. 3068–3072, Nov. 2023.
- [19] Y. Liu, Y. Ye, and R. Q. Hu, "Secrecy outage probability in backscatter communication systems with tag selection," *IEEE Wireless Communications Letters*, vol. 10, no. 10, pp. 2190–2194, Oct. 2021.
- [20] Y. Zhang, Y. Dang, M. Kaveh, Z. Yan, R. Jäntti, and Z. Han, "Physical layer challenge-response authentication between ambient backscatter devices," *IEEE Transactions on Information Forensics and Security*, doi: 10.1109/TIFS.2026.3655191, 2026.
- [21] X. Guo, et al., "Efficient ambient LoRa backscatter with on-off keying modulation," *IEEE/ACM Transactions on Networking*, vol. 30, no. 2, pp. 641–654, Apr. 2021.
- [22] Y. Chu, et al., "RSS-based multiple co-channel sources localization with unknown shadow fading and transmitted power," *IEEE Transactions on Vehicular Technology*, vol. 71, no. 12, pp. 13344–13355, 2022.
- [23] D. L. Galappaththige, F. Rezaei, C. Tellambura, and S. Herath, "RIS-empowered ambient backscatter communication systems," *IEEE Wireless Communications Letters*, vol. 12, no. 1, pp. 173–177, 2023.
- [24] X. Xu, et al., "Simultaneous information and power transfer under a non-linear RF energy harvesting model," in *Proc. IEEE Int. Conf. Commun. Workshops (ICC Workshops)*, May 2017, pp. 179–184.